

Climatic variations during the Holocene inferred from radiocarbon and stable carbon isotopes in a high-alpine cave

Caroline Welte^{1,2}, Jens Fohlmeister^{3,4}, Melina Wertnik^{1,2}, Lukas Wacker¹, Bodo Hattendorf⁵, Timothy I. Eglinton², Christoph Spötl⁶

¹ Laboratory of Ion Beam Physics, ETHZ, Otto-Stern Weg 5, 8093 Zurich, Switzerland,

² Geological Institute, ETHZ, Sonnegstrasse 5, 8092 Zurich, Switzerland

³ Potsdam Institute for Climate Impact Research, Telegrafenberg, 14473 Potsdam, Germany

⁴ GFZ German Research Centre for Geosciences, Section 'Climate Dynamics and Landscape Development', 14473 Potsdam, Germany

⁵ Laboratory of Inorganic Chemistry, D-CHAB, ETHZ, Vladimir-Prelog Weg 1, 8093 Zurich, Switzerland

⁶ Institute of Geology, University of Innsbruck, Innrain 52f, 6020 Innsbruck, Austria

Keywords: radiocarbon, stable carbon isotopes, LA-AMS, speleothems, high-alpine cave

Correspondence to: Caroline Welte: cwelte@phys.ethz.ch, Jens Fohlmeister: jens.fohlmeister@pik-potsdam.de

Formatted: English (United Kingdom)

Abstract

Rapid and continuous analysis of radiocarbon (^{14}C) concentration in carbonate samples at very high spatial resolution has been made possible with the new LA-AMS (laser ablation accelerator mass spectrometry) technique. A novel technique making use of laser ablation coupled online to accelerator mass spectrometry (LA-AMS) allows analyzing the radiocarbon (^{14}C) concentration in carbonate samples continuously at high spatial resolution within very short analysis times. This new technique novel approach can provide radiocarbon data at a spatial resolution similar to the spatial resolution that of stable carbon (C) isotope measurements by isotope-ratio mass spectrometry (IRMS) and, thus, can help to interpret $\delta^{13}\text{C}$ signatures, which otherwise are difficult to understand due to numerous processes contributing to changes in C-isotope changes-ratios. In this work, we analyzed $\delta^{13}\text{C}$ and ^{14}C on the Holocene stalagmite SPA 127 from the high-alpine Spannagel Cave (Austria). Both proxies respond in a complex manner with respect to climate variability. Combined stable carbon and radiocarbon profiles allow to identify three growth periods characterized by different $\delta^{13}\text{C}$ signatures: (i) the period 8.5 to >8.0 ka BP is characterized by relatively low $\delta^{13}\text{C}$ values with small variability combined with a comparably high radiocarbon reservoir effect (expressed as dead carbon fraction, dcf) of around 60%. This points towards C contributions of host rock dissolution and/or from an "old" organic matter (OM) reservoir in the karst potentially mobilized due to the warm climatic conditions of the early Holocene. (ii) Between 3.8–8 and 3.8 ka BP a strong variability in $\delta^{13}\text{C}$ reaching values from -8 to +1‰ with a generally lower dcf was observed. The $\delta^{13}\text{C}$ variability is most likely caused by changes in gas exchange processes in the cave, which are induced by reduced drip rates as derived from reduced stalagmite growth rates. Additionally, the lower dcf indicates that the OM reservoir is contributed less to stalagmite growth in this period possibly as a result of reduced meteoric precipitation or because it is/was exhausted. (iii) In the youngest section between 2.4–3.8 and 2.4 ka BP, comparably stable and low $\delta^{13}\text{C}$ values combined with an increasing dcf reaching up to 50% are again hinting towards a contribution of an aged OM reservoir in the karst. This study reveals the enormous high potential of combining high-density-resolution ^{14}C profiles in speleothems with $\delta^{13}\text{C}$ records for in order to disentangling climate-related C dynamics above caves in karst systems.

1 Introduction

Understanding the climate of the past is the key for understanding how climate and environment will change in the future. Insights into paleoclimate are gained through the study of archives with stalagmites being a prominent example for a terrestrial archive. Stalagmites can grow continuously over thousands to tens of thousands of years (Cheng et al., 2016; Fairchild et al., 2006; Moseley et al., 2020). Caves hosting stalagmites are present on all continents (with the possible exception of except Antarctica) and uranium-series disequilibrium dating allows to build robust chronologies (Richards and Dorale, 2003; Scholz and Hoffmann, 2008). Trace-element and stable isotope data of stalagmites allow the reconstruction of climatic conditions in the past. For example, the oxygen isotope composition ($\delta^{18}\text{O}$) is generally interpreted as a combination of a temperature and a meteoric precipitation signal (Lachniet, 2009; Wackerbarth et al., 2010). The interpretation of the stable carbon isotope signature ($\delta^{13}\text{C}$), however, is more challenging since additional local effects, such as vegetation changes (e.g., Bar-Matthews et al., 1999; Denniston et al., 2007; Fohlmeister et al., 2020), the carbonate dissolution mechanism (e.g., (e.g., Fohlmeister et al., 2010b; Lechleitner et al., 2016),-) and in-cave fractionation processes (e.g., (e.g., Matthey et al., 2016; Spotl et al., 2005)) may have an influence and little is known about the relative magnitude of these processes. Besides the stable C isotopes, radiocarbon (^{14}C) decaying with a half-life of ~5700 yrs (Kutschera,

2013)(Kutsehera, 2013) can be a valuable tool in speleothem research (e.g., (e.g., Bajo et al., 2017; Lechleitner et al., 2016)). So far, this isotope has not been fully exploited in speleothem sciences, mostly due to the time-consuming sampling and processing as well as the comparably high costs associated with these analyses. However, recently both issues have been considerably improved by invention (Welte et al., 2016a; Welte et al., 2016b) and advances in Laser-Ablation coupled to Accelerator mass Spectrometry (LA-AMS; (LA-AMS; Welte et al., 2017; Yeman et al., 2019)Welte et al., 2016a,b), which can be well applied to carbonate material.

In most karst systems, dissolution of the carbonate host rock is driven by soil-derived carbonic acid. In this case, the two major soil-derived C sources contributing to the $\delta^{13}\text{C}$ values of the speleothem are pedogenic CO_2 from the degradation of soil organic matter (SOM) and root respiration that acidifies the meteoric water as it percolates through the soil and the karst rock. Recently, evidence was found for an additional C source stemming from CO_2 derived from the oxidation of old organic matter (OM) in the deep vadose zone. If a radiocarbon-independent chronology for the stalagmite exists, the dead carbon fraction (def) can be derived through comparison of the measured ^{14}C profile in the stalagmite ($F^{14}\text{C}_{\text{stal}}$) with the ^{14}C atmosphere's signature ($F^{14}\text{C}_{\text{atm}}$) of the same time Genty and Massault (1997):

$$\text{def} = \left(1 - \frac{F^{14}\text{C}_{\text{stal}}}{F^{14}\text{C}_{\text{atm}}}\right) \cdot 100\% \quad (1)$$

Values can range from a few % up to 70% and commonly vary within a single speleothem with time. The magnitude of the def is influenced by multiple factors, such as the age of soil OM, contributing to soil gas CO_2 production (Fohlmeister et al., 2011b) and consequently altering the ^{14}C concentration in the stalagmite. Also the CO_2 partial pressure ($p\text{CO}_2$) in the soil plays an important role, with a complex relationship between the amount of soil gas $p\text{CO}_2$ and the def (Fohlmeister et al., 2011b). Additionally, the conditions of karst dissolution, i.e. open vs. closed system, affect the def. In a more open system, the def is low because the percolating water can continuously exchange C with the soil gas CO_2 leading to a ^{14}C concentration in the stalagmite that is dominated by the near-atmospheric soil ^{14}C signature. Fractionation and gas exchange processes in the cave are also potential candidates for modulation of the def. These main factors driving the def in turn are influenced by numerous parameters such as hydrological and environmental conditions above the cave. Several studies (e.g.,) showed that during periods of increased rainfall the def is enhanced, which is explained by either accelerated SOM decomposition rates and the resulting increased mean age of soil gas CO_2 or, more likely, by a shift towards more closed system conditions under higher precipitation regimes.

An increasing number of cave systems are reported where carbonate dissolution occurs even if no significant soil layers exists above the cave. Acidic conditions in the seepage water are achieved via oxidation of pyrite or other sulfide minerals disseminated in the bedrock. In this case the C isotope composition in the drip water is dominated by the bedrock, and the def is therefore expected to be relatively high (>50%). Under those conditions the $\delta^{13}\text{C}$ values of the speleothems reflect those levels of the bedrock, i.e. are shifted closer towards 0‰ compared to more depleted $\delta^{13}\text{C}$ values of speleothem CaCO_3 of around -12 and -10‰, for cave systems with a soil and vegetation cover. An overview of relevant processes as well as the resulting def and $\delta^{13}\text{C}$ are summarized in .

Table 1 Summary of expected $\delta^{13}\text{C}$ and $\delta^{18}\text{O}$ values in stalagmite CaCO_3 for different dominant processes. Note, that in natural samples often a mixture of these processes with different proportions contributed to the stalagmite, which complicates the interpretation.

Process		Expected* $\delta^{13}\text{C}$ (‰)	Expected* $\delta^{18}\text{O}$ (‰)
Carbonate dissolution via carbonic acid	open-system	$< -10\text{‰}$	Comparably low, i.e. around -10‰
	closed-system	$> -10\text{‰}$	Comparably high, i.e. close to -50‰
Carbonate dissolution via oxidation of pyrite		Close to 0‰	Very high, i.e. $> 50\text{‰}$
Old OM contribution to seepage water acidification		Shift to more negative values	Shift towards higher values ($> 50\text{‰}$ possible)

Thus we investigated a

The studied stalagmite by means of C isotope systematics that under study grew in the high-alpine Spannagel cave system (Tyrol, Austria), a high-alpine cave system (Tyrol, Austria; Spötl et al., 2004) by means of C isotope systematics. This high-alpine cave system that was investigated in many studies in the context of palaeoclimate and palaeoenvironmental research mostly using O isotopes and growth phases as proxies (e.g., Fohlmeister et al., 2013; Spötl and Mangini, 2010). The gneiss covering the cave-bearing marble contains interspersed fine-crystalline pyrite and is topped by a thin soil layer with sparse vegetation. It was hypothesized that the oxidation of pyrite contributes considerably to the dissolution of the host-rock marble and, hence, to the growth of stalagmites and flowstones, in particular during cold climate periods when there is no soil present at this high altitude (Spötl and Mangini, 2007). During some interglacials including the Holocene, when alpine soils are present in the catchment of the cave's drip water, sulfide oxidation and soil-derived CO_2 may operate in tandem. Consequently, the stable C isotope signal of stalagmites from this cave is expected to be complex.

The aim of this study is to gain deeper insights into the climatically driven C dynamics in this cave by highly spatially resolved in-situ ^{14}C analyses of a Holocene stalagmite. This study takes advantage of the recently introduced method of laser ablation coupled to accelerator mass spectrometry (LA-AMS) (Welte et al., 2016a; Welte et al., 2016b), which reaches a similar spatial resolution as micro-milling for stable isotope analysis (e.g., Spötl and Matthey, 2006). Using the combined ^{14}C and $\delta^{13}\text{C}$ records measured in this study as well as the previously published $\delta^{18}\text{O}$ signal (Fohlmeister et al., 2013), we explore the key processes influencing the carbon isotope composition of speleothems in this cave and gain a better understanding of the potential and limits of ^{14}C analysis of carbonates using LA-AMS.

2 Radiocarbon and dead carbon fraction

In most karst systems, dissolution of the carbonate host rock is driven by soil-derived carbonic acid. In this case, the two major soil-derived C sources contributing to the $\delta^{13}\text{C}$ values of the speleothem are pedogenic CO_2 from the degradation of soil organic matter (SOM) and root respiration that acidifies the meteoric water as it percolates through the soil and the karst rock. Recently, evidence was found for an potential additional C source stemming from CO_2 derived from the oxidation of "old" organic matter (OM) in the deep vadose zone (Bergel et al., 2017;

Noronha et al., 2015). The water charged with carbonic acid charged water then dissolves the host rock CaCO_3 . All of those C-pools have different characteristics with respect to ~~its~~their stable and radiocarbon isotope systematissignatures (Figure 1) (Fig. X).

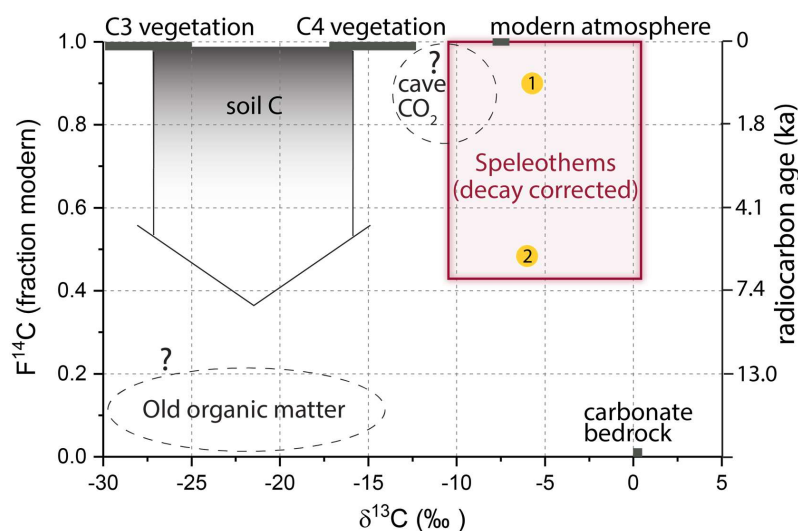


Figure 1: Carbon isotopic signatures of carbon-bearing reservoirs in karst systems. Yellow circles mark speleothem-C resulting from different ~~scenari~~processes: 1. CaCO_3 dissolution via soil- CO_2 -derived carbonic acid. 2. Deep OC contribution to seepage water feeding speleothems (adapted from Fairchild and Baker (2012)).

Fig. X

When working with radiocarbon in speleothems it is important to determine the reservoir effect (Genty and Massault, 1997) (Genty and Massault, 1997). If a radiocarbon-independent chronology for the stalagmite exists, the reservoir effect, which is often termed dead carbon fraction (dcf), can be derived through comparison of the measured ^{14}C profile in the stalagmite ($F^{14}\text{C}_{\text{stal}}$) with the ^{14}C atmosphere's signature ($F^{14}\text{C}_{\text{atm}}$) of the same time (Genty and Massault (1997)):

$$dcf = \left(1 - \frac{F^{14}\text{C}_{\text{stal}}}{F^{14}\text{C}_{\text{atm}}}\right) \cdot 100\% \quad (1)$$

Values for dcf can range from a few % up to 70% (Bajo et al., 2017; Southon et al., 2012) and commonly vary within a single speleothem with time (Bajo et al., 2017; Noronha et al., 2014; Therre et al., 2020). The magnitude of the dcf is influenced by multiple factors, such as the age of soil OM, contributing to soil gas CO_2 production (Fohlmeister et al., 2011b) and consequently altering the ^{14}C concentration in the stalagmite. Also the CO_2 partial pressure ($p\text{CO}_2$) in the soil plays an important role, with a complex relationship between the amount of soil gas $p\text{CO}_2$ and the dcf (Fohlmeister et al., 2011b). Additionally, the conditions of karst dissolution, i.e. open vs. closed system (Fohlmeister et al., 2011a; Hendy, 1971), affect the dcf. In a more open system, the dcf is low because the percolating water can continuously exchange C isotopes with the soil gas CO_2 leading to a ^{14}C concentration in the stalagmite that is dominated by the near-atmospheric soil ^{14}C signature (Southon et al., 2012) (Southon et al., 2012). In a more closed system, this exchange is inhibited with the extreme case being a completely closed system,

where for each mole of carbonic acid one mole of CaCO_3 is dissolved resulting in a dcf of up to 50%. Fractionation and gas exchange processes in the cave are also potential candidates for modulation of the dcf. These main factors driving the dcf in turn are influenced by numerous parameters such as hydrological and environmental conditions above the cave. Several studies (e.g., Bajo et al., 2017; Fohlmeister et al., 2010a; Griffiths et al., 2012; Lechleitner et al., 2016; Noronha et al., 2014) showed that during periods of increased rainfall the dcf in the stalagmite is enhanced. A likely explanation is a shift towards more closed-system conditions (see-) under higher meteoric precipitation regimes. It was argued, that under more humid (arid) conditions the pore spaces in soils are clogged with (devoid of) water, leaving less (more) opportunity for C-exchange processes between dissolved inorganic C species and soil gas CO_2 (Fohlmeister et al., 2010).

An increasing number of cave systems are have been reported where carbonate dissolution occurs even if no significant soil layers exists above the cave, indicating climatic conditions, less suited for the existence of vegetation cover. Acidic conditions in the seepage water are achieved via oxidation of pyrite or other sulfide minerals disseminated in the bedrock (Bajo et al., 2017; Lauritzen, 2001; Spotl et al., 2016). In this case the C isotope composition in the drip water is dominated by the bedrock, and the dcf is therefore expected to be relatively high (>50%). Under those conditions the $\delta^{13}\text{C}$ values of the speleothems reflect those of the (marine-derived) bedrock, i.e. are shifted closer to 0‰ compared to lower $\delta^{13}\text{C}$ values of speleothem CaCO_3 of around -12 to -10‰, for cave systems with a soil and vegetation cover. An overview of relevant processes as well as the resulting dcf and $\delta^{13}\text{C}$ are summarized in .

Field Code Changed

Table 1 Simplified summary of expected $\delta^{13}\text{C}$ (assuming C3 vegetation cover) and dcf values in stalagmite CaCO_3 for different dominant processes. In many karst systems various combinations of these processes complicate the interpretation.

Field Code Changed

Process		Expected $\delta^{13}\text{C}$ (‰)	Expected dcf (%)
<u>Carbonate dissolution via carbonic acid</u>	open-system	< -10‰	Comparably low, i.e. around 10%
	closed-system	> -10‰	Comparably high, i.e. close to 50%
<u>Carbonate dissolution via oxidation of pyrite</u>		Close to 0‰	Very high, i.e. > 50%
<u>“Old” OM contribution to seepage water acidification</u>		< -10‰	Shift towards higher values (> 50% possible)

3 Materials & Methods

3.1 Sample

Spannagel cave is located in the Tux Valley (47.08028°N, 11.67167°E; Zillertal Alps, western Austria) and opens at 2531 m above sea level. It forms a more than 12 km-long system of galleries and short shafts, which developed in a Jurassic marble tectonically overlain by gneiss. This superposition does not only allow for high-precision U-series dating of stalagmites (due to their relatively high U contents), but also gives rise to carbonate dissolution via sulfuric acid stemming from pyrite oxidation. The thin alpine soil coverage provides an additional pedogenic source of acidity and the interplay between the two processes is reflected by highly variable stable C isotope values as well as dcf in Spannagel speleothems. Stalagmite SPA 127 was found in-situ in the eastern part of the cave system, which was never ice-covered during the Holocene (Fohlmeister et al., 2013). The stalagmite grew from

8.45 to 2.24 ka BP with an average growth rate of approximately 25 $\mu\text{m/a}$ as confirmed by nine U/Th-ages (Fohlmeister et al., 2013). There is no macro- and microscopic evidence for the existence of hiatuses in this specimen. Further evidence for the absence of hiatuses is provided by two additional speleothems, SPA12 and SPA128, from the same cave are partly coeval with SPA 127. These additional speleothems have a higher dating density in parts, where SPA 127 has only a few radiometric U-Th dating points and also do not show evidence of hiatuses (Fohlmeister et al., 2013). In combination with the well replicated stable O isotope signals we are confident; that the growth of SPA 127 was not affected by hiatuses.

The 15 cm-long polished slab of the stalagmite analyzed in this study was first used for stable oxygen and carbon isotope analysis where sampling was performed along the extension axis. For LA-AMS analysis, the same section was used but broken in two pieces at a distance from top (dft) of approximately 10 cm, which will be referred to as “top piece” and “bottom piece”.

3.2 Stable isotope analysis

Subsamples for stable carbon isotope analysis were micromilled at 100 μm increments and measured using an automated online carbonate preparation system linked to a triple collector gas source mass spectrometer (Delta^{plus}XL, ThermoFisher, Bremen, Germany) at the University of Innsbruck. Values are reported relative to the Vienna Pee Dee Belemnite standard. The long-term precision of the $\delta^{13}\text{C}$ values (1 σ standard deviation of replicate analyses) is 0.06‰ (Spötl, 2011). The respective $\delta^{18}\text{O}$ values have been published earlier (Fohlmeister et al., 2013).

3.3 Radiocarbon analysis using LA-AMS

By focusing a laser on the surface of a solid sample at sufficiently high energy densities, a small portion of material is ablated and can be used for trace element or isotopic analysis allowing for fast and spatially resolved analysis (Gray, 1985; Koch and Gunther, 2011). ^{14}C analysis of SPA 127 was performed by LA coupled with AMS (Welte et al., 2016a; Welte et al., 2017). For this study, a slightly modified LA-AMS setup was used reaching a smaller spot size (75x140 μm^2) and higher energy densities of up to 8 J/cm² allowing for increased signal intensities, i.e. ^{12}C -currents. With LA-AMS a quasi-continuous data stream is produced at 10 sec intervals in the AMS. This is the minimal integration time of the AMS and together with the laser spot width d and the scanning velocity v defines the spatial resolution R according to $R = d + v \cdot 10 \text{ sec}$.

LA-scans were placed as close as possible to the stable isotope tracks in order to facilitate matching between the two data sets (Fig. 24). However, the LA-AMS setup does not permit to place laser tracks close to the rim of samples causing an offset between the two sampling lanes of approximately 5 mm. Speleothem growth layers are often curved, resulting in a potential offset between stable isotope and radiocarbon data of up to several hundred micrometers, with the outer LA-scan appearing somewhat older than the stable isotope record. Since the curvature of the growth layers is most likely variable, a constant correction factor cannot be has not been applied.

On the “top piece” of SPA 127 two subsequent scans in opposite direction were performed, first from young to old (T1) and then vice versa (T2) on the same track with a scanning velocity of 20 $\mu\text{m/s}$ and a laser energy density of approximately 5 J/cm². On the “bottom piece” a total of three analyses were performed: the initial scan from old to young (B1: 10 $\mu\text{m/s}$, 1-2 J/cm²) was followed by a second repeated scan from bottom to top (B2: old to young, 25 $\mu\text{m/s}$, 8 J/cm²) after removing the top ~0.5 mm of the sample surface by mechanical polishing. The second scan was necessary to ensure that the unusual ^{14}C signature observed in the oldest part of the stalagmite during the first scan (see section “Results”) was not the result of a potentially contaminated surface. A final third

Formatted: English (United States)

analysis (B3) consisting of two scans performed in opposite directions was performed at 20 $\mu\text{m/s}$ and 5 J/cm^2 . Processing of the raw ^{14}C data was performed using in-house standards also analyzed by LA-AMS for blank subtraction and standard normalization (marble, $F^{14}\text{C} = 0$ and coral standard, $F^{14}\text{C} = 0.9445 \pm 0.0018$). A Savitzky-Golay (SG) filter is applied to the recorded ^{14}C signal of B3, which is a smoothing method that reduces noise while maintaining the shape and height of peaks (Savitzky and Golay, 1964). In brief, a polynomial is fitted to a sub-set of the data points and evaluated at the center of the approximation interval. Two parameters, namely the number of points defining the approximation interval and the maximum polynomial order, can be defined. The smoothing has been applied to the two sub-scans of B3 (from “old to young” and vice versa) as well as to the combined data to ensure robustness of the filter. Corresponding uncertainties are estimated from the square root of the sum of the squared difference between the measured $F^{14}\text{C}$ value and the SG fit at each point within the interval. This value is then divided by the square root of the difference between the interval length (number of data points) and the maximum order allowed for the polynomial, which is equivalent to the degree of freedom.

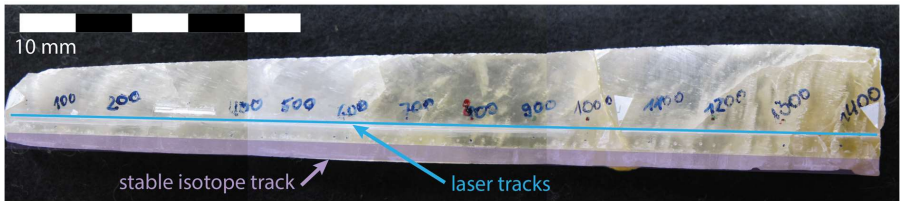


Figure 2-1 Polished slab of SPA 127 (top left). Top and bottom piece (green box indicates bottom slab) with location of the stable isotope track marked in purple and LA-AMS test track in blue (the tracks corresponding to the data presented in this work were placed next to the test tracks). The total length of the slab is 14.6 cm. The green box shows the bottom piece after removal of approximately 0.5 mm from the sample surface with the repeated LA-AMS laser track and approximate locations (green areas) of layers exhibiting anomalies during LA-AMS.

Fourier Transform Infrared spectroscopy (FTIR) analysis

Fourier Transform Infrared spectroscopy (FTIR) is a standard non-invasive technique for material analysis. The coupling of the IR spectrometer with a microscope enables micro analysis, while the development of focal plane array (FPA) detectors allowed to upgrade point measurements to imaging. Attenuated total reflection (ATR) is a sampling technique, which requires no sample preparation other than a flat surface and is independent of the thickness of the sample as it is performed upon contact of the sample with the ATR crystal, which is a medium of high refractive index.

The analysis of the speleothem was performed on a Spotlight 400 FT-IR Imaging System (Perkin Elmer, Massachusetts, USA), equipped with a MCT array (mercury cadmium telluride) detector. The stalagmite was placed under the microscope on a motorized stage and focused to measure the spectrum between 4000 and 520 cm^{-1} using a micro-ATR objective germanium crystal at 4 cm^{-1} spectral resolution and 32 scans. The detection area of a measurement was 300 x 200 μm^2 in diameter (spot size). An area of 1.9 x 3.4 mm in the vicinity of the abnormal $^{14}\text{C}/^{12}\text{C}$ behavior observed by LA-AMS was selected for rastering by FTIR (Fig. A1).

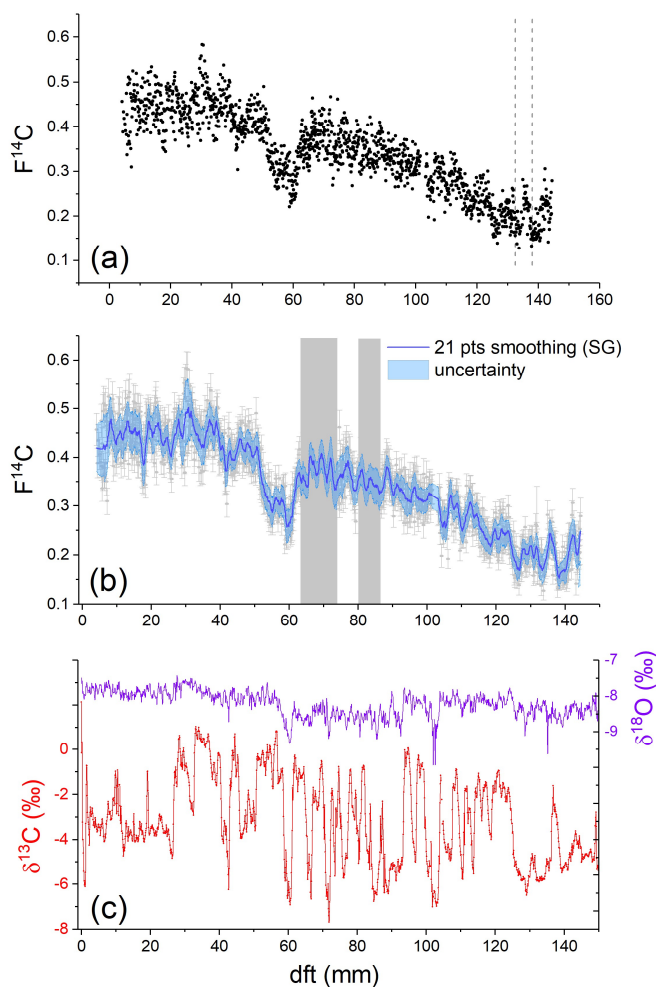


Fig. 2 (A) $F^{14}C$ profile of SPA 127 plotted without error bars for reasons of clarity. Grey dashed lines indicate two locations potentially contaminated with epoxy resin (details in SI, Figs 3 and 4). (B) $F^{14}C$ profile including error bars corresponding to measurement precision (grey) with an overlain SG filter of 21 points interval width with a maximum polynomial degree of 2. The grey shaded areas represent depths in which the quality check for the SG filter was not satisfactory (compare Fig. A1). Details can be found in the text. (C) $\delta^{13}C$ and $\delta^{18}O$ signal of SPA 127.

4 Results

4.1 Dead carbon fraction

1. Radiocarbon

^{14}C results for both pieces of SPA_127 (T1, T2 and B3) are reported as dcf (blue line in Fig. 3 a and shown in AFig. S8 a), where error bars are not displayed for reasons of clarity. The measured $F^{14}C$ ranges from about 0.55 at the top to approximately 0.15 towards the oldest part of the stalagmite. Between 0 and ca. 40 mm, the $F^{14}C$ varies around a comparably constant value of 0.45, followed by a pronounced dip between 40 mm and 70 mm. From 70 mm to 140 mm, the $F^{14}C$ decreases from 0.4 to 0.2. The measurement precision is approximately 8% for

the younger slab and 10% for the older piece with a spatial resolution of 280 μm per data point. In B, $F^{14}\text{C}$ data is depicted in grey with uncertainties corresponding to the analytical error. In order to reduce noise a SG filter has been applied with an interval length of 21 points and the polynomial order of 2.

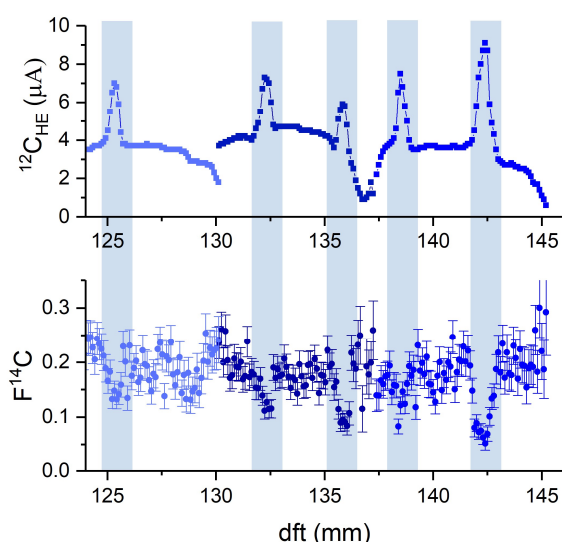


Fig. 3 Anomalies observed in the signal intensity ($^{12}\text{C}_{\text{HE}}$) and $F^{14}\text{C}$ for the initial scan performed on the bottom piece. The scan consists of three sub-scans represented by the different shades of blue. At the beginning and towards the end of each sub-scan the $^{12}\text{C}_{\text{HE}}$ current rises and drops respectively, i.e. at 130 mm, 137 mm and 145 mm, which is an expected behavior. The anomalies in both measurement parameters are indicated by the blue boxes.

An unexpected signal was observed in the bottom piece as shown in . The signal intensity (top panel) recorded for the bottom section of SPA-127 showed five peaks with corresponding $F^{14}\text{C}$ dips. The repeated scan (B2), which was performed after removal of the top surface layer showed a similar behavior (see Fig. A3). We additionally investigated the regions showing these peaks with FTIR. These anomalies are less distinctly observed in the third LA-AMS scan (see Fig.s A2 and Fig. A4). A detailed description can be found in the SI.

2.1. Dead carbon fraction

From the ^{14}C profile (B), the Stal-Age (Scholz and Hoffmann, 2011) age-depth model was applied to previously published U-Th data (Fohlmeister et al., 2013) and the known ^{14}C content of the atmosphere during the Holocene (Reimer et al., 2016), and the def was calculated according to equation (1) for the more than 1500-1402 radiocarbon data points (Figure 3Fig. 4 A). Again, a SG filter was applied (interval: 21, maximum polynomial order: 2) and for comparison the $\delta^{18}\text{O}$ and $\delta^{13}\text{C}$ data are shown in the same graph (Figure 3Fig. 4 a and bB). The U-Th-dates and the corresponding average growth rate calculated in using Stal-Age (Scholz and Hoffmann, 2011) are displayed in Figure 3Fig. 4 cC.

4.2 Stable C isotopes

The previously published $\delta^{18}\text{O}$ values (Fohlmeister et al., 2013) and unpublished $\delta^{13}\text{C}$ data (this study) are shown in Figure 3Fig. 4 (a and b, respectively). A large amplitude and fast changes ranging from -8‰ to +1‰ characterize

Formatted: Font: 10 pt

Formatted: Font: 10 pt

Formatted: Font: 10 pt

Formatted: Font: 10 pt

$\delta^{13}\text{C}$ throughout the entire length of the speleothem but are especially pronounced between 30 and 130 mm. Layers exhibiting a comparably stable $\delta^{13}\text{C}$ occur at the top and bottom of SPA 127, specifically ranging from 0 to 25 mm and from 125 to 150 mm.

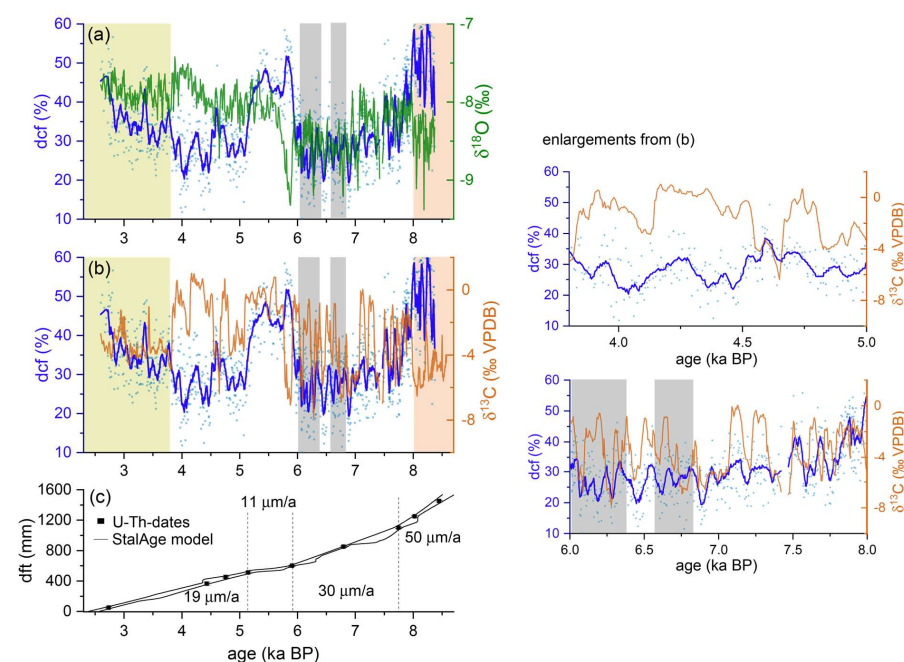


Figure 3:4 Dcf (light blue dots) with a 21 point SG filter (dark blue line) plotted against age and compared to (A) $\delta^{18}\text{O}$ (green line) (Fohlmeister et al., 2013) and (B) $\delta^{13}\text{C}$ (orange line). The yellow, white and orange shaded areas represent phases with distinct stable isotope-and-dcf characteristics. Details can be found in the text. Light grey shaded areas mark regions where the SG filter was determined with lower confidence. Enlargements of this graph are shown in the right panel. (C) Growth history of SPA 127 obtained by StalAge applied to dated depths (black squares, errors are smaller than the symbol size). Numbers represent average growth rates of the individual sections.

3. FTIR measurements

In the regions where LA-AMS anomalies were observed, two different types of matrices were revealed by the FTIR spectra (Fig. A2), representing calcite and epoxy resin. The epoxy resin spectra were found for measurement points along a crack present in this area. The calcite matrix was found in all other measurement points outside of the crack.

4. Stable C isotopes

The $\delta^{13}\text{C}$ and previously published $\delta^{18}\text{O}$ values (Fohlmeister et al., 2013) are shown in C. A large amplitude and fast changes ranging from -8‰ to +1‰ characterize $\delta^{13}\text{C}$ throughout the entire length of

the speleothem but are especially pronounced between 30 and 130 mm. Depths exhibiting a comparably stable $\delta^{13}\text{C}$ are found at the top and bottom of SPA 127, specifically ranging from 0 to 25 mm and from 125 to 150 mm.

5 Discussion

The interpretation of the results on C isotopes in SPA 127 will be divided in ~~three~~four main parts ~~that correspond to three sections identified on the speleothem~~ ~~through~~based on their distinct $\delta^{13}\text{C}$ characteristics. ~~first the anomalies in ^{14}C and ^{13}C current observed in the bottom part will be discussed followed by a detailed discussion on carbon isotope evolution. For this task we subdivided the stalagmite into three sections, which were identified to underlie different dynamics.~~

1. LA-AMS anomalies in the old section of SPA 127 (> 8 ka BP, > 120 mm)

The five ^{12}C current peaks correlating with strongly depleted F^{14}C observed between 120 and 145 mm depth, i.e. from 8.0 to 8.4 ka BP indicating that these layers are composed of a different material than the bulk. The higher ^{12}C currents are associated with a matrix that converts more readily into CO/CO_2 upon LA compared to CaCO_3 , a behavior that is known for organic substances with a higher oxygen/carbon stoichiometric ratio (Frick and Gunther, 2012). In order to ascertain whether the substance in these layers is inherent to the stalagmite or a contamination, its exact composition has been determined using FTIR. These measurements revealed that the anomalies were caused by epoxy resin (Fig. A2 and A3).

Indeed, the stalagmite was glued in this section after it broke into two parts shortly after its removal in 2002 CE. Although the speleothem was only glued on one location, we observed the glue at least at five positions. Those observations fall in line with small cracks. This suggests, that the glue was able to soak relatively long distances through those small cracks. Hence, attention should be paid when working with glued speleothems, especially, if the type of geochemical analyses is based on methods not easily able to differentiate the analyzed material such as e.g. laser ablation IRMS (Spotl and Matthey, 2006), while e.g. IRMS based on drilled material, which is acidified by H_3PO_4 , should be unaffected.

These findings underline that unlike conventional analytical methods applied to stalagmite samples for ^{14}C analysis, which provide exclusively the isotope composition of the CaCO_3 , LA-AMS additionally yields the ^{14}C content of OM captured in stalagmites. Despite the fact that this offers novel possibilities it also requires particular caution to distinguish between inherent OM and contaminants of organic origin.

^{14}C data used for interpretation of SPA 127 stem from scan B3, which was largely unaffected from the epoxy because the scan was placed off the glued joint as confirmed by conventional ^{14}C analysis (see Fig. A4).

5.1 Old section of SPA 127 (≈ 8.5 -8.0 ka BP)

In the oldest part of SPA 127, the dcf is comparably high ($\sim 60\%$), while $\delta^{13}\text{C}$ is relatively depleted with values ~~smaller~~ lower than -5‰ on average. Although the reservoir effect is extremely high, in principle the obtained C-isotope composition can be explained without a major contribution of pyrite oxidation. The relatively low $\delta^{13}\text{C}$ value actually contradicts this mode of host rock dissolution but is in line with a sparse C3 vegetation ($\delta^{13}\text{C} \approx -25\text{‰}$) above the cave and ~~nearly completely closed carbonate host rock~~ dissolution ~~under nearly closed~~ conditions

of the host rock (compare Figure 4 Fig. 5 C and D). The stoichiometry of CaCO_3 dissolution by carbonic acid predicts that only about half of the C in the solution comes is derived from the host rock under nearly completely closed conditions. Under the reasonable assumption Given that the $\delta^{14}\text{C}$ of the Jurassic host rock is devoid of ^{14}C is 0, the biogenic component must be older than the contemporaneous atmosphere to allow dcf values larger than 50%. Thus, in addition to living vegetation, which contributes atmospheric radiocarbon, an "old" OM source, which respire radiocarbon-depleted CO_2 , is required to explain depleted $\delta^{13}\text{C}$ values and elevated dcf. Such "old" OM is also argued to have contributed to the radiocarbon reservoir effect of Moomi Cave (Socotra Island) during the last glacial period (Therre et al., 2020). Observations from other cave and karst systems also point to important C pools deep in the vadose karst, e.g., (Benavente et al., 2010; Bergel et al., 2017; Breecker et al., 2012). Nevertheless, in a high elevation and in a sparsely vegetated high elevation region, this is the first finding of that this kind.

Formatted: Font: 10 pt

The speleothem growth phase prior to 8.0 ka falls coincides with the early Holocene thermal maximum, which is also reflected by the depleted $\delta^{18}\text{O}$ values hinting towards higher temperatures (Fohlmeister et al., 2013; Mangini et al., 2005). Warmer periods likely favor microbial organic decomposition of, e.g., OM present in the epikarst below the soil zone, which leads to an increase in pCO_2 and, hence, more acidic water. In turn, more CaCO_3 can be dissolved resulting giving rise to in higher speleothem growth rates, which is indeed observed in this growth period of the speleothem (Figure 3 Fig. 4, orange shaded area). Thus, growth rate and the C-isotope composition of stalagmite SPA 127 are in agreement with the presence of a deep OM reservoir in the karst system above the cave. Indeed this phase falls in the period of the early Holocene thermal maximum, which is also reflected by the depleted $\delta^{18}\text{O}$ values hinting towards warmer temperatures (Mangini et al., 2005; Fohlmeister et al., 2013).

Formatted: Font: 10 pt

5.2 Rapid changes in dcf and stable C isotopes (3.8 to 8.0 to 3.8 ka BP)

The growth rate was reduced in this period compared to the previous one (Fig. 3). This either suggests, that meteoric precipitation or the amount of soil-derived C was reduced, both resulting in a smaller amount of dissolved carbonate species transported to the cave. The low $\delta^{13}\text{C}$ values of the first growth period were superseded by rapid and very large variations of $\delta^{13}\text{C}$. This pattern is complex and its interpretation is difficult, as this behavior has not been observed elsewhere. Processes in the soil and karst as well as in-cave processes have to be taken into consideration. High-resolution LA-AMS ^{14}C measurements in conjunction with O isotope data and growth rate changes, however, greatly assist in disentangling the driving mechanism(s) for these $\delta^{13}\text{C}$ variations in the C time series. The dcf between 3.8 and 8.0 and 3.8 ka BP is generally lower than in the older section. This means that either, the aged OM in the karst was depleted or its degradation was reduced, possibly due to a reduction in meteoric precipitation (as deduced from growth rate reduction). Both reasons, less meteoric precipitation and a depleted deep OM pool, would well explain the observed reduction in growth rate. The only speleothem C sources available in this period were consequently the close-to-modern SOM and the radiocarbon-free host rock.

The dcf record shows a strong and rapid increase around 6 ka and a rapid decrease back to pre-6 ka levels at around 5 ka (Fig. 43). The increase in dcf occurs at the same time as a significant decrease in $\delta^{18}\text{O}$, but dcf remains elevated when $\delta^{18}\text{O}$ jumps back again shortly after. Instead, the decrease in dcf at 5 ka occurs contemporaneously with a $\delta^{13}\text{C}$ decrease after $\delta^{13}\text{C}$ values remained at elevated values for nearly a millennium. The reason for such a behavior of the dcf remains elusive. In this section

387 , we focus on ~~the causing cause of~~ the large and rapid jumps in $\delta^{13}\text{C}$ ~~value in this interval~~ by testing two hypotheses.

388 **Hypothesis 1:** ~~processes~~ Processes above the cave, i.e. different carbonate dissolution processes, cause the rapid
389 switching

390 Two different processes may have caused carbonate dissolution at Spannagel cave in this period. The first ~~is~~
391 ~~involves from~~ soil CO_2 - CO_2 -derived carbonic acid, ~~while The the~~ second ~~process is operates via from~~ sulfuric
392 acid formed ~~through by~~ pyrite oxidation (compare ~~Figure 4~~ ~~Fig. 4~~ ~~Fig. 5~~ A and B). During times when the first
393 process dominates, the stable carbon isotopic composition ~~in of the~~ stalagmites is strongly influenced by C from
394 the soil shifting ~~the~~ $\delta^{13}\text{C}$ towards more negative values. At the same time, the dcf is expected to be relatively low
395 (at least <50%) as the comparably ^{14}C -rich soil C contributes significantly to the signal. In contrast, pyrite oxidation
396 leads to more positive $\delta^{13}\text{C}$ values in the stalagmite corresponding to the $\delta^{13}\text{C}$ composition of the host rock, as the
397 $\delta^{13}\text{C}$ - $\delta^{13}\text{C}$ -depleted biogenic source contributes little or even no C (Bajo et al., 2017; Spotl et al., 2016). Under
398 these conditions, the dcf should increase to values close to 100% if the comparably modern soil contribution is
399 absent. If the observed $\delta^{13}\text{C}$ variations are caused by rapid alternation between both processes, a positive
400 correlation between $\delta^{13}\text{C}$ and the dcf has to be expected, with extreme values in the dcf as outlined above. However,
401 no significant long-lasting term, ~~signifieant~~ positive correlation for the two data series, i.e. $\delta^{13}\text{C}$ and dcf, is observed
402 (~~compare~~ Fig. S10) and ~~the~~ extreme DCF values ~~are are~~ not ~~detected~~ observed. A robust comparison of both data
403 sets is impeded because of the different spatial offset of the two measurement tracks from the growth axis. The
404 radiocarbon track is located ca. 5 mm further from the central growth axis than the stable isotope track (Figure
405 2 ~~Fig. 1~~). Growth layers cannot be ~~seen~~ identified, but the small stalagmite diameter suggests steeply sloping
406 dipping layers resulting in an apparent shift of the dcf towards older ages relative to ~~the~~ $\delta^{13}\text{C}$. Indeed, such a delay
407 is observable when comparing details in the two data series (Figure 3 ~~Fig. 4~~ b). Taking a potential offset between
408 the two records into account (see Materials & Methods ~~See. Methods. 3~~), a positive correlation between main
409 features ~~the in~~ $\delta^{13}\text{C}$ and dcf are observable for the middle period, especially between ~~6-8~~ and ~~8-6~~ ka BP and also
410 partly between 5 and 3.8 and ~~5-3~~ ka BP. Those phases are interrupted by the phase interval of the previously described
411 strong increase in dcf.

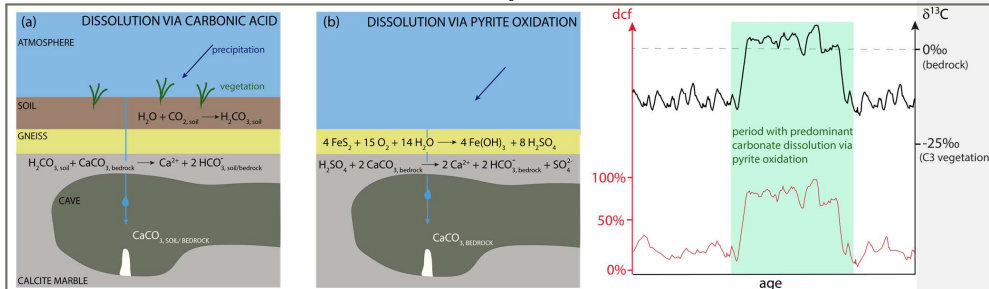
412

Formatted: Font: 10 pt

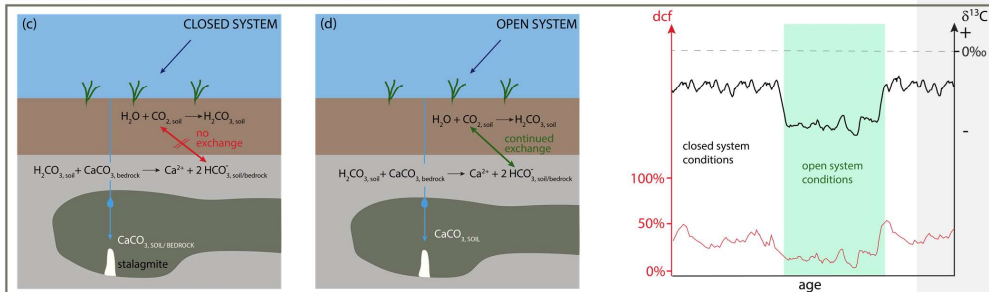
Formatted: Font: 10 pt

Formatted: Font: 10 pt

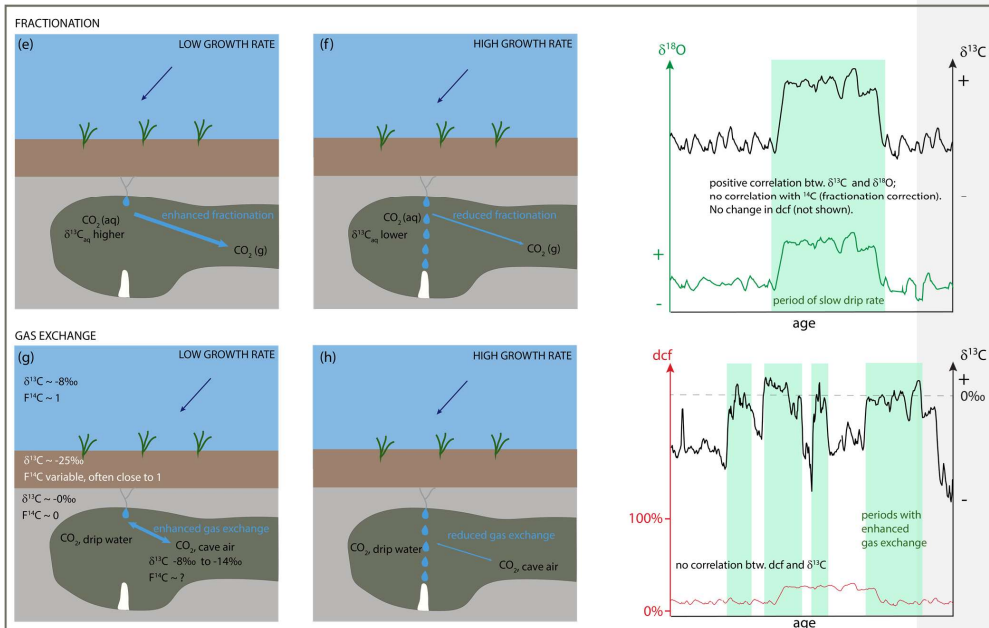
CARBONATE DISSOLUTION MECHANISM ALTERNATING BETWEEN SOIL CO₂ AND SULFIDE OXIDATION



CARBONATE DISSOLUTION MECHANISM: OPEN vs. CLOSED



PROCESSES IN CAVE: FRACTIONATION



413

414
415

Figure 4-5 Overview of different processes that can influence $\delta^{14}\text{C}$ and $\delta^{13}\text{C}$ in speleothems. Details For details can be found in the text.

However, here we want to elaborate on what is causing the large and rapid jumps in $\delta^{13}\text{C}$ -value in this interval. Here we test two hypotheses.

2.—Rapid changes in $\delta^{13}\text{C}$ and stable C isotopes (3.8 to 8 ka BP)

As indicated by the reduced growth rate in SPA 127 (–), the climate shifted towards a regime with reduced precipitation. The low $\delta^{13}\text{C}$ -values of the first growth period are superseded by rapid and very large variations. This $\delta^{13}\text{C}$ -pattern is complex and its interpretation is difficult, as this behavior has not been observed elsewhere. Processes in the soil and karst above the cave as well as in cave processes have to be taken into consideration. High-resolution LA-AMS- ^{14}C measurements in conjunction with O isotope data and growth rate changes, however, greatly assist in disentangling the driving mechanism(s) for the variations in the C time series. The $\delta^{13}\text{C}$ between 3.8 and 8 ka BP is generally lower than in the older section, as the additional source for carbonic acid from the old OM in the karst is most likely strongly reduced either due to the possible reduction in precipitation (as deduced from growth rate reduction) or that the aged OM reservoir was depleted. The only C sources in this period are close to modern SOM and the radiocarbon-free host rock.

Hypothesis 1: processes above the cave, i.e. different carbonate dissolution processes, cause the rapid switching. Two different processes may have caused carbonate dissolution at Spannagel cave in this period, i.e. (i) via carbonic acid formed from soil CO_2 derived and (ii) due to sulfuric acid from pyrite oxidation (compare A and B). During times when the first process dominates, the stable carbon isotopic composition in the stalagmite is strongly influenced by C from the soil shifting the $\delta^{13}\text{C}$ towards more negative values. At the same time, the $\delta^{13}\text{C}$ is expected to be relatively low (at least <50%) as the comparably- ^{14}C -rich soil C contributes to the signal. In contrast, pyrite oxidation leads to more positive $\delta^{13}\text{C}$ in the stalagmite corresponding to the $\delta^{13}\text{C}$ composition of the host rock, as the $\delta^{13}\text{C}$ -depleted biogenic source contributes little or even no C. Under these conditions, the $\delta^{13}\text{C}$ should increase to values close to 100% if the modern soil contribution is absent. If the observed $\delta^{13}\text{C}$ -variations are caused by rapid alternation between both processes, a positive correlation between $\delta^{13}\text{C}$ and the $\delta^{13}\text{C}$ has to be expected, with extreme values in the $\delta^{13}\text{C}$ as outlined above. However, no long-lasting, significant positive correlation for the two data series, i.e. $\delta^{13}\text{C}$ and $\delta^{13}\text{C}$, is observed (compare Fig A7) and the extreme DCF values are not detected. A robust comparison of both data sets is impeded because of the different spatial offset of the two measurement tracks from the growth axis. The radiocarbon track is located ca. 5 mm further from the central growth axis than the stable isotope track (–). Growth layers cannot be seen, but the small stalagmite diameter suggests steeply sloping layers resulting in an apparent shift of the $\delta^{13}\text{C}$ towards older ages relative to the $\delta^{13}\text{C}$. Indeed, such a delay is observable when comparing details in the two data series (– b). Since the curvature of the growth layers is most likely variable, a constant correction factor cannot be applied. Taking these alignment difficulties into account (see See Methods.3), a positive correlation between main features the $\delta^{13}\text{C}$ and $\delta^{13}\text{C}$ are observable for the middle period, especially between 3.8–5 ka and 6 and 8 ka BP and also partly between 3.8 and 5 ka. Those phases are interrupted by the phase of the previously described strong increase in $\delta^{13}\text{C}$.

The large $\delta^{13}\text{C}$ swings in $\delta^{13}\text{C}$ suggest frequent switches a change between the carbonate dissolution mechanisms from carbonic acid dissolution to pyrite oxidation. However, this is expected to be accompanied by an increase of the $\delta^{13}\text{C}$ to 100% because of the diminishing ^{14}C -rich soil signature, which, however, is not observed. Generally, the $\delta^{13}\text{C}$ is even smaller than in the youngest and oldest sections of the stalagmite, i.e. before/after 3.8 ka and after/before 8 ka BP. The correlation between $\delta^{13}\text{C}$ and $\delta^{13}\text{C}$ suggests that there might have been a change

between the open to-and closed carbonate dissolution conditionsregimes, but the magnitude of $\delta^{13}\text{C}$ variations found in SPA 127 is larger than if triggered by this process even when changing from a completely open to a completely closed system (Hendy, 1971; Fohlmeister et al., 2011). Thus, additional processes in the cave most likely caused this unusual behavior and the high-magnitude and high-frequency $\delta^{13}\text{C}$ variations.

• **Hypothesis 2:** processes-Processes in the cave cause the rapid switching

A major factor influencing the carbon isotope composition of stalagmites are fractionation processes (compare Figure 4Fig-5 E and F), which occur during degassing of CO_2 and precipitation of CaCO_3 from the solution. Fast dripping results in fast growth and leaves less time for fractionation processes- or C isotope exchange (compare Figure 4Fig-5 G and H) and vice versa (e.g., Fohlmeister et al., 2018; Scholz et al., 2009). In addition, the difference in pCO_2 between water and cave-air CO_2 can also influence isotope fractionation and C exchange processes. In the middle part of SPA 127, the average growth rate decreased to $\leq 30 \mu\text{m/a}$, which is significantly lower than in the oldest section. As discussed earlier, the reduction in growth rateis might have been partly induced by reduced meteoric precipitation resulting in slower drip rates and-reduced-growthor by reduced soil or karst CO_2 concentrations leading to less dissolved host rock CaCO_3 . In addition, a lower or absent contribution of an “old” OM reservoir in the karst would have led to a lower pCO_2 difference between the CO_2 concentration in the drip water and cave air, which favors an increase in $\delta^{13}\text{C}$ through fractionation and C isotope exchange processes in the cave. We hypothesize that the rapid changes in $\delta^{13}\text{C}$ might correlate with short-seale-term changes in growth rate, which cannot be resolved by the available U-Th chronology, enabling or disabling isotope processes-in-the-cave, i.e. (i)-fractionation and (ii)-gas exchange in the cave that are described in the following two paragraphs.

(i) Changes in fFractionation effects

During periods of slow growth, fractionation processes can significantly alter the isotopic composition of the stalagmite. During CO_2 degassing from the drip water, the lighter molecules echange-are preferentially transferred into the gas phase, resulting in a solution leaving-solution-behind-that-is enriched in heavy isotopes. This-is-valid-for- ^{13}C -and- ^{14}C -isotopes. Indeed, recent experiments (Fahrni et al., 2017) support earlier findings that fractionation of radiocarbon relative to ^{12}C is about twice as large as for ^{13}C relative to ^{12}C (Stuiver and Robinson, 1974). However, as radiocarbon measurements are corrected for fractionation effects via $\delta^{13}\text{C}$ values, it is impossible to detect a potential correlation between the two isotopes due to fractionation effects. However, potential fractionation effects-affecting $\delta^{13}\text{C}$ also affect-influences $\delta^{18}\text{O}$ and can be verified confirmed by a positive correlation between stable C isotopes and O isotopes, e.g.- (Dreybrodt, 2008; Polag et al., 2010). Applying a running correlation coefficient between $\delta^{13}\text{C}$ and $\delta^{18}\text{O}$ is a powerful tool to detect fractionation changes through time (Fohlmeister et al., 2017). The-11-point running correlation coefficients calculated for the two time series of SPA 127 show no stalagmite sections with a high correlation coefficient, but vary without any obvious pattern between -1 and +1 (compare Fig. S10A7, bottom panel). Thus, fractionation was most likely not the main process causing the large variations in $\delta^{13}\text{C}$, but may have played a minor role during some periods.

(ii) Prior calcite precipitation (PCP)

Formatted: Font: 10 pt

Formatted: Font: 10 pt

PCP can have an effect on $\delta^{13}\text{C}$, even a large ones as observed for our stalagmite. While this would not have an effect on ^{14}C , we would expect that $\delta^{18}\text{O}$ should show a similar behavior, which is not the case. Thus, we can safely assume, that PCP is not responsible for the rapid changes observed in SPA 127.

(iii) Gas exchange processes

Another process that is a potential candidate for causing the behavior observed in SPA 127 in this interval is the C isotope exchange between CO_2 of the cave air and C dissolved in the drip water. These gas exchange processes may be dominant if the stalagmite growth rate is sufficiently low. C exchange between CO_2 of the cave air and C dissolved in the drip water and when. This becomes important if drip intervals are long and/or the differences between the $p\text{CO}_2$ of the water and cave air is small (Hendy, 1971; Scholz et al., 2009). In this case, the C isotopic composition of the drip water when reaching the top of the stalagmite depends mainly on the initial $\delta^{13}\text{C}$ of drip water and on the degree of C isotope exchange with the cave atmosphere. Spannagel Cave is well ventilated throughout the year with cave air $\delta^{13}\text{C}$ values of -10 to -11‰ (Tochterle et al., 2017), which is significantly lighter-lower than that of the atmosphere, i.e. approximately -8‰ (Keeling et al., 2010). These more negative values are a hint towards a contribution from soil air to the cave air, reaching the cave through cracks in the bedrock. The following assumptions were made: the $\delta^{13}\text{C}$ of drip water is composed of two biogenic C sources ($\delta^{13}\text{C} \sim -25\text{‰}$) and host rock ($\delta^{13}\text{C} \sim +2.80\text{‰}$) and about 20 - 30% are derived from the host rock (based on the dcf in this interval). Accounting for about 10‰ to 11‰ fractionation between soil gas CO_2 and HCO_3^- during the transition of soil gas CO_2 to dissolved inorganic carbon (DIC), the initial drip water, which was feeding the stalagmite, has had a $\delta^{13}\text{C}$ value between -11.52 and -9.44‰ (Mook et al., 1974). Considering progressing-Rayleigh fractionation effects in the cave, carbonate $\delta^{13}\text{C}$ values of -8‰ appear feasible (Scholz et al., 2009, Deininger et al., 2012) without any exchange of C isotopes. C isotope exchange processes lead to water significantly enriched in ^{13}C . When cave air $\delta^{13}\text{C}$ values around -11‰ exchanges with drip water, the C isotopic composition of the water will increase, as the transition of gaseous CO_2 to HCO_3^- involves a fractionation of about +10 to +11‰ at temperatures between 0 and 5°C. Thus, drip water in C isotopic equilibrium with cave air CO_2 , which is the most extreme case, should have $\delta^{13}\text{C}$ values of -1 to 0‰. Precipitation of CaCO_3 from such water would result in $\delta^{13}\text{C}$ values of around 0 to +1‰ as observed for some short periodsintervals.

Similar assumptions-considerations regarding the cave air with respect to $\delta^{13}\text{C}$ can be applied to radiocarbon. If the cave ventilation is sluggish, $F^{14}\text{C}$ in the cave air will deviate from atmospheric values (i.e. $F^{14}\text{C}_{\text{atm}} \approx 1$) as it is influenced by other sources, such as transferred-soil air or degassed- CO_2 degassed from drip water, which both are depleted with respect to atmospheric values. In a recent study, cave air has been shown to be depleted in radiocarbon with values as low as $F^{14}\text{C} \approx 0.6$ (Minami et al., 2015). When the cave ventilation is not effectively changing the depleted radiocarbon towards more atmospheric values, C isotope exchange processes are not detectable from-using ^{14}C in speleothems. As isotopic fractionation is not important for radiocarbon (as explained above), C isotope exchange of DIC with cave air, which both have a similar radiocarbon content, would have no effect on the ^{14}C signal of the precipitated calcite.

In summary, combined high-resolution $\delta^{13}\text{C}$ and radiocarbon measurements are a valuable tool to shed new light on processes affecting C isotopes in the subsurface. Using well justified assumptions and first-order calculations

of mixing and fractionation effects, in-cave C isotope-exchange processes remain the only explanation for the rapid and high-magnitude $\delta^{13}\text{C}$ anomalies changes

5.3 Interpretation of dcf and $\delta^{13}\text{C}$ in the youngest section of SPA 127 (2.5 to 3.8 to 2.5 ka BP)

In the youngest section of this stalagmite a behavior similar to the oldest section with respect to $\delta^{13}\text{C}$ and radiocarbon content is observed. From approximately 3.8 ka BP onward, the dcf increases slowly from about 20% to 50%. Correspondingly, $\delta^{13}\text{C}$ shows a lower variability than in the middle part with mean $\delta^{13}\text{C}$ values of -3‰ to -4‰, which is also comparable to the behavior observed for the interval > 8 ka BP. As $\delta^{13}\text{C}$ is does not showing any long-term trend as observed for the reservoir effect, we rule out a change to more closed carbonate dissolution conditions driving the increase in dcf. The only explanation that can lead to such an increase is the development of an “old” C reservoir. We propose that climatic conditions have changed such that this “old” OM pool in the karst, which is was decoupled from the atmosphere, is being has become the main OM derived CO_2 source, been successively contributed CO_2 . This CO_2 resulted in acidification in a comparable way as soil CO_2 enhancing carbonate dissolution and ultimately contributed to stalagmite CaCO_3 . The isotopic $\delta^{14}\text{C}$ imprint, however, is significantly different to soil CO_2 causing the observed increase in dcf. Between approximately 8 and 6 ka BP the Alps experienced a warmer climate than today (Ivy-Ochs et al., 2009; Nicolussi et al., 2005). A study conducted by Nicolussi et al. (2005) in the Kauner valley, situated approximately 70 km west of Spannagel Cave, showed that the timberline was significantly higher during that period (Figure SFig-5) supporting a warmer climate. Between 6 and 4 ka BP the timberline was comparable with to the present-day situation.

Formatted: Font: 10 pt

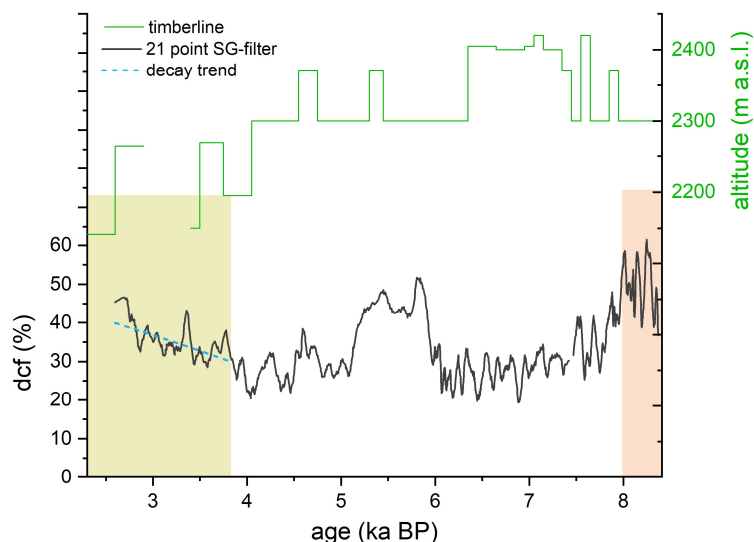
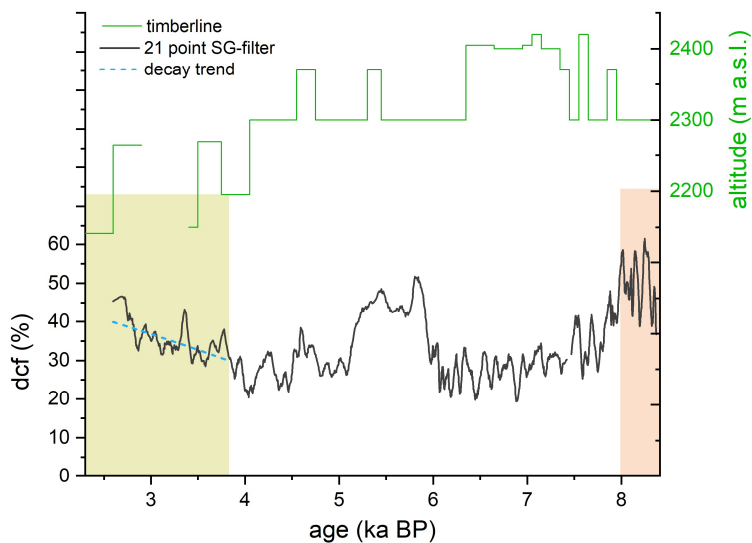


Figure 56 Comparison of the dcf in stalagmite SPA 127 with the elevation of the timberline reconstructed for the nearby-Kauner valley 70 km west of Spannagel Cave (green line, after Nicolussi et al. (2005)) with the dcf. Around 4 ka BP the timberline starts-started to decline which is concurrent with an increase in dcf, i.e., a decrease in initial $\delta^{14}\text{C}$. This decrease closely follows a radiocarbon decay trend (dashed blue line). Green and red areas mark the three different time periods as indicated in Figure 3Fig-4.

556

557 It is expected that with the lowering of the timberline after ~4 ka the vegetation density decreased as well, which
 558 should be reflected in the ~~eave-carbonates~~speleothem $\delta^{13}\text{C}$ values. This, however, is not the case during this
 559 period pointing towards a relatively stable contribution of ~~organic-soil~~-derived CO_2 . Possibly, a certain proportion
 560 of plants that grew during the early to mid-Holocene warm epoch died and the corresponding OM located in the
 561 deeper vadose zone was initially stabilized due to reduced ~~meteoric~~ precipitation and later became mobilized due
 562 to enhanced microbial activity. Considering the low mean annual temperatures at ~~the-this~~ high-alpine site,
 563 decomposition processes are most likely slow, allowing OM to ~~ageing~~ during decomposition as indicated in a
 564 recent study by Shi et al. (2020)-. The radiocarbon composition of the ageing SOM will closely follow a
 565 ~~radioearbon-radiocarbon~~-specific exponential decay and is responsible for ~~a-the depleting-depleted~~ radiocarbon
 566 ~~concentration in~~ soil gas CO_2 . Depending on the contribution of root-respired CO_2 of ~~Alpine living~~ plants (~~grasses,~~
 567 ~~alpine-mats~~) compared to the decomposed CO_2 ~~of-from~~ dead OM, the initial $\text{F}^{14}\text{C}_{\text{dcf}}$ will closely follow an
 568 exponential decay, resembling that of the radiocarbon decay and thus would contribute to the observed increase of
 569 the dcf. The closer the observed ~~indecrease~~ in the initial $\text{F}^{14}\text{C}_{\text{dcf}}$ follows that of ~~a~~ radiocarbon decay trajectory,
 570 the larger the contribution of CO_2 from the ageing SOM reservoir ~~in relation to root-respired~~ CO_2 . Based on the
 571 observed rate of ~~indecrease~~ in ~~dcfinal~~ F^{14}C , which compares well with the radiocarbon decay trend (~~blue dashed~~
 572 ~~line in Figure 5~~), we suggest that the majority of CO_2 -DIC that contributed to the speleothem CaCO_3 ~~must-have~~
 573 had its origin in ~~ageing-aged~~ soil OM.

Formatted: Font: 10 pt



574

575 *Fig. 6 Comparison of the timberline reconstruction of the nearby Kauner valley (green line, after Nicolussi et al. (2005)) with*
 576 *the initial F^{14}C , i.e. the ^{14}C present in the respective layer at the time when it formed SPA-127. Around 4 ka BP the timberline*
 577 *starts to decline which is concurrent with a decrease in initial F^{14}C . This decrease closely follows a radiocarbon decay trend*
 578 *(blue line). Green and red areas mark the three different time periods as indicated in-.*

6 Conclusion

Combined stable carbon isotope and radiocarbon ~~analysis~~~~analyses~~ of stalagmite SPA_127 provide a comprehensive picture ~~on of~~ the carbon dynamics at the ~~high-alpine~~ Spannagel Cave. Due to the novel LA-AMS technique, a high-ly spatially resolved ^{14}C time series ~~allowed~~~~allows~~ unprecedented insights into processes in this ~~high-alpine~~ karst system. Care has to be taken when applying LA-AMS to stalagmites as epoxy resin used in sample preparation leads to distorted results.

~~Results from this study allow to distinguish three intervals with different carbon dynamics~~~~Key findings of this study for the three periods characterized by different C dynamics:~~

- (i) ~~The interval before~~ > 8 ka BP ~~is characterized by~~ generally low and stable $\delta^{13}\text{C}$ values combined with a comparably high dcf ($>50\%$) pointing towards the existence of an “old” OM reservoir in the ~~epi~~karst ~~rock~~. ~~CO_2 emanating from this presaged C pool, which~~ provides additional carbonic acid ~~potentially enhancing and enhances~~ bedrock dissolution.
- (ii) ~~The interval between 8 and 3.8~~ $8-3.8$ ka BP ~~this period~~ is characterized by a strong variability in $\delta^{13}\text{C}$ with a generally lower dcf suggesting that the “old” OM reservoir in the karst had either been exhausted or stabilized (less production to aged respired soil/karst CO_2) possibly due to reduced ~~meteoric~~ precipitation. This is supported by a lower stalagmite growth rate in this period. In-cave gas exchange processes are the most likely explanation for the strong $\delta^{13}\text{C}$ variability, as (i) bedrock dissolution mechanisms, i.e. pyrite oxidation vs. carbonic acid dissolution, are not supported by the magnitude of changes in dcf and stable C, even though the temporal coherence indicates that some of the $\delta^{13}\text{C}$ variations might be explained by the bedrock dissolution mode (open vs. closed carbonate dissolution system) and, (ii) fractionation processes in the cave cannot explain the large shifts as no correlation between $\delta^{18}\text{O}$ and $\delta^{13}\text{C}$ is observed.
- (iii) ~~In the interval between 3.8 and 2.4~~ $3.8-2.4$ ka BP: the comparably more stable $\delta^{13}\text{C}$ signature combined with an increasing dcf hints towards a contribution ~~of from~~ an ageing OM reservoir in the karst similar to the period > 8 ka BP. This OM reservoir contributed to the stalagmite growth in this period due to warmer climatic conditions. While the contribution of “old” OM in the oldest growth phase was stable, the youngest section indicates an ageing of this ~~OM~~ reservoir.

Author contribution

CW, JF and CS conceptualized the content of this manuscript. CW, MW, BH carried LA-AMS measurements out, CS conducted stable carbon isotope analyses. MW and LW developed the data reduction strategy. JF, CW and TE interpreted the data and compared them to published records. CW prepared the manuscript with contributions from all co-authors.

Competing interests

The authors declare that they have no conflict of interest.

Acknowledgements

JF acknowledges support from DFG grants FO 809/2-1 and FO 809/4-1. MW was supported by an ETH Research Grant (03 18-2). FTIR analyses were performed by Laura Hendriks. We also thank the two reviewers who helped to improve this manuscript.

618 References

- 619 Bajo, P., Borsato, A., Drysdale, R., Hua, Q., Frisia, S., Zanchetta, G., Hellstrom, J., and Woodhead, J.:
620 Stalagmite carbon isotopes and dead carbon proportion (DCP) in a near-closed-system situation: An
621 interplay between sulphuric and carbonic acid dissolution, *Geochimica Et Cosmochimica Acta*, 210,
622 208-227, 2017.
- 623 Bar-Matthews, M., Ayalon, A., Kaufman, A., and Wasserburg, G. J.: The Eastern Mediterranean
624 paleoclimate as a reflection of regional events: Soreq cave, Israel, *Earth and Planetary Science Letters*,
625 166, 85-95, 1999.
- 626 Benavente, J., Vadiillo, I., Carrasco, F., Soler, A., Linan, C., and Moral, F.: Air Carbon Dioxide Contents in
627 the Vadose Zone of a Mediterranean Karst, *Vadose Zone Journal*, 9, 126-136, 2010.
- 628 Bergel, S. J., Carlson, P. E., Larson, T. E., Wood, C. T., Johnson, K. R., Banner, J. L., and Breecker, D. O.:
629 Constraining the subsoil carbon source to cave-air CO₂ and speleothem calcite in central Texas,
630 *Geochimica Et Cosmochimica Acta*, 217, 112-127, 2017.
- 631 Breecker, D. O., Payne, A. E., Quade, J., Banner, J. L., Ball, C. E., Meyer, K. W., and Cowan, B. D.: The
632 sources and sinks of CO₂ in caves under mixed woodland and grassland vegetation, *Geochimica Et*
633 *Cosmochimica Acta*, 96, 230-246, 2012.
- 634 Cheng, H., Edwards, R. L., Sinha, A., Spotl, C., Yi, L., Chen, S., Kelly, M., Kathayat, G., Wang, X., Li, X.,
635 Kong, X., Wang, Y., Ning, Y., and Zhang, H.: The Asian monsoon over the past 640,000 years and ice age
636 terminations, *Nature*, 534, 640-646, 2016.
- 637 Denniston, R. F., DuPree, M., Dorale, J. A., Asmerom, Y., Polyak, V. J., and Carpenter, S. J.: Episodes of
638 late Holocene aridity recorded by stalagmites from Devil's Icebox Cave, central Missouri, USA,
639 *Quaternary Research*, 68, 45-52, 2007.
- 640 Dreybrodt, W.: Evolution of the isotopic composition of carbon and oxygen in a calcite precipitating
641 H₂O-CO₂-CaCO₃ solution and the related isotopic composition of calcite in stalagmites, *Geochimica*
642 *et Cosmochimica Acta*, 72, 4712-4724, 2008.
- 643 Fahrni, S. M., Southon, J. R., Santos, G. M., Palstra, S. W., Meijer, H. A., and Xu, X.: Reassessment of the
644 ¹³C/¹²C and ¹⁴C/¹²C isotopic fractionation ratio and its impact on high-precision radiocarbon dating,
645 *Geochimica et Cosmochimica Acta*, 213, 330-345, 2017.
- 646 Fairchild, I. J. and Baker, A.: *Speleothem science: from process to past environments*, John Wiley &
647 Sons, 2012.
- 648 Fairchild, I. J., Smith, C. L., Baker, A., Fuller, L., Spotl, C., Matthey, D., McDermott, F., and Eimp:
649 Modification and preservation of environmental signals in speleothems, *Earth-Science Reviews*, 75,
650 105-153, 2006.
- 651 Fohlmeister, J., Arps, J., Spotl, C., Schroder-Ritzrau, A., Plessen, B., Gunter, C., Frank, N., and Trussel,
652 M.: Carbon and oxygen isotope fractionation in the water-calcite-aragonite system, *Geochimica Et*
653 *Cosmochimica Acta*, 235, 127-139, 2018.
- 654 Fohlmeister, J., Kromer, B., and Mangini, A.: The Influence of Soil Organic Matter Age Spectrum on the
655 Reconstruction of Atmospheric C-14 Levels Via Stalagmites, *Radiocarbon*, 53, 99-115, 2011a.
- 656 Fohlmeister, J., Plessen, B., Dudashvili, A. S., Tjallingii, R., Wolff, C., Gafurov, A., and Cheng, H.: Winter
657 precipitation changes during the Medieval Climate Anomaly and the Little Ice Age in arid Central Asia,
658 *Quaternary Science Reviews*, 178, 24-36, 2017.
- 659 Fohlmeister, J., Scholz, D., Kromer, B., and Mangini, A.: Modelling carbon isotopes of carbonates in
660 cave drip water, *Geochimica Et Cosmochimica Acta*, 75, 5219-5228, 2011b.
- 661 Fohlmeister, J., Schroder-Ritzrau, A., Spotl, C., Frisia, S., Miorandi, R., Kromer, B., and Mangini, A.: The
662 Influences of Hydrology on the Radiogenic and Stable Carbon Isotope Composition of Cave Drip Water,
663 *Grotta Di Ernesto (Italy)*, *Radiocarbon*, 52, 1529-1544, 2010a.
- 664 Fohlmeister, J., Schroeder-Ritzrau, A., Spoetl, C., Frisia, S., Miorandi, R., Kromer, B., and Mangini, A.:
665 The influences of hydrology on the radiovenic and stable carbon isotope composition of cave drip
666 water, *Grotta die Ernesto (Italy)*, *Radiocarbon*, 52, 1529-1544, 2010b.

667 Fohlmeister, J., Voarintsoa, N. R. G., Lechleitner, F. A., Boyd, M., Brandtstatter, S., Jacobson, M. J., and
 668 Oster, J. L.: Main controls on the stable carbon isotope composition of speleothems, *Geochimica Et*
 669 *Cosmochimica Acta*, 279, 67-87, 2020.
 670 Fohlmeister, J., Vollweiler, N., Spotl, C., and Mangini, A.: COMNISPA II: Update of a mid-European
 671 isotope climate record, 11 ka to present, Holocene, 23, 749-754, 2013.
 672 Frick, D. A. and Gunther, D.: Fundamental studies on the ablation behaviour of carbon in LA-ICP-MS
 673 with respect to the suitability as internal standard, *Journal of Analytical Atomic Spectrometry*, 27,
 674 1294-1303, 2012.
 675 Genty, D. and Massault, M.: Bomb C-14 recorded in laminated speleothems: Calculation of dead
 676 carbon proportion, *Radiocarbon*, 39, 33-48, 1997.
 677 Gray, A. L.: Solid Sample Introduction by Laser Ablation for Inductively Coupled Plasma Source-Mass
 678 Spectrometry, *Analyst*, 110, 551-556, 1985.
 679 Griffiths, M. L., Fohlmeister, J., Drysdale, R. N., Hua, Q., Johnson, K. R., Hellstrom, J. C., Gagan, M. K.,
 680 and Zhao, J. X.: Hydrological control of the dead carbon fraction in a Holocene tropical speleothem,
 681 *Quat. Geochronol.*, 14, 81-93, 2012.
 682 Hendy, C. H.: The isotopic geochemistry of speleothems—I. The calculation of the effects of different
 683 modes of formation on the isotopic composition of speleothems and their applicability as
 684 palaeoclimatic indicators, *Geochimica et cosmochimica Acta*, 35, 801-824, 1971.
 685 Ivy-Ochs, S., Kerschner, H., Maisch, M., Christl, M., Kubik, P. W., and Schluchter, C.: Latest Pleistocene
 686 and Holocene glacier variations in the European Alps, *Quaternary Science Reviews*, 28, 2137-2149,
 687 2009.
 688 Keeling, R., Piper, S., Bollenbacher, A., and Walker, S.: Monthly atmospheric $^{13}\text{C}/^{12}\text{C}$ isotopic ratios
 689 for 11 SIO stations, Trends: a compendium of data on global change, 2010. 2010.
 690 Koch, J. and Gunther, D.: Review of the state-of-the-art of laser ablation inductively coupled plasma
 691 mass spectrometry, *Appl Spectrosc*, 65, 155-162, 2011.
 692 Kutschera, W.: Applications of accelerator mass spectrometry, *International Journal of Mass*
 693 *Spectrometry*, 349, 203-218, 2013.
 694 Lachniet, M. S.: Climatic and environmental controls on speleothem oxygen-isotope values,
 695 *Quaternary Science Reviews*, 28, 412-432, 2009.
 696 Lauritzen, S.-E.: Marble stripe karst of the Scandinavian Caledonides: an end-member in the contact
 697 karst spectrum, *Slovenska akademija znanosti in umetnosti*, 2001.
 698 Lechleitner, F. A., Baldini, J. U. L., Breitenbach, S. F. M., Fohlmeister, J., McIntyre, C., Goswami, B.,
 699 Jamieson, R. A., van der Voort, T. S., Prufer, K., Marwan, N., Culleton, B. J., Kennett, D. J., Asmerom, Y.,
 700 Polyak, V., and Eglinton, T. I.: Hydrological and climatological controls on radiocarbon concentrations
 701 in a tropical stalagmite, *Geochimica Et Cosmochimica Acta*, 194, 233-252, 2016.
 702 Mangini, A., Spötl, C., and Verdes, P.: Reconstruction of temperature in the Central Alps during the
 703 past 2000 yr from a $\delta^{18}\text{O}$ stalagmite record, *Earth and Planetary Science Letters*, 235, 741-751, 2005.
 704 Matthey, D. P., Atkinson, T. C., Barker, J. A., Fisher, R., Latin, J. P., Durrell, R., and Ainsworth, M.: Carbon
 705 dioxide, ground air and carbon cycling in Gibraltar karst, *Geochimica Et Cosmochimica Acta*, 184, 88-
 706 113, 2016.
 707 Minami, M., Kato, T., Horikawa, K., and Nakamura, T.: Seasonal variations of ^{14}C and $\delta^{13}\text{C}$ for cave
 708 drip waters in Ryugashi Cave, Shizuoka Prefecture, central Japan, *Nuclear Instruments and Methods in*
 709 *Physics Research Section B: Beam Interactions with Materials and Atoms*, 362, 202-209, 2015.
 710 Mook, W. G., Bommerson, J. C., and Staverman, W. H.: Carbon Isotope Fractionation between
 711 Dissolved Bicarbonate and Gaseous Carbon-Dioxide, *Earth and Planetary Science Letters*, 22, 169-176,
 712 1974.
 713 Moseley, G. E., Spotl, C., Brandtstatter, S., Erhardt, T., Luetscher, M., and Edwards, R. L.: NALPS19: sub-
 714 orbital-scale climate variability recorded in northern Alpine speleothems during the last glacial period,
 715 *Climate of the Past*, 16, 29-50, 2020.
 716 Nicolussi, K., Kaufmann, M., Patzelt, G., van der Plicht, J., and Thurner, A.: Holocene tree-line variability
 717 in the Kauner Valley, Central Eastern Alps, indicated by dendrochronological analysis of living trees and
 718 subfossil logs, *Vegetation History and Archaeobotany*, 14, 221-234, 2005.

719 Noronha, A. L., Johnson, K. R., Hu, C. Y., Ruan, J. Y., Southon, J. R., and Ferguson, J. E.: Assessing
 720 influences on speleothem dead carbon variability over the Holocene: Implications for speleothem-
 721 based radiocarbon calibration, *Earth and Planetary Science Letters*, 394, 20-29, 2014.
 722 Noronha, A. L., Johnson, K. R., Southon, J. R., Hu, C. Y., Ruan, J. Y., and McCabe-Glynn, S.: Radiocarbon
 723 evidence for decomposition of aged organic matter in the vadose zone as the main source of
 724 speleothem carbon, *Quaternary Science Reviews*, 127, 37-47, 2015.
 725 Polag, D., Scholz, D., Mühlinghaus, C., Spotl, C., Schroder-Ritzrau, A., Segl, M., and Mangini, A.: Stable
 726 isotope fractionation in speleothems: Laboratory experiments, *Chemical Geology*, 279, 31-39, 2010.
 727 Reimer, P. J., Bard, E., Bayliss, A., Beck, J. W., Blackwell, P. G., Ramsey, C. B., Buck, C. E., Cheng, H.,
 728 Edwards, R. L., Friedrich, M., Grootes, P. M., Guilderson, T. P., Hafliðason, H., Hajdas, I., Hatté, C.,
 729 Heaton, T. J., Hoffmann, D. L., Hogg, A. G., Hughen, K. A., Kaiser, K. F., Kromer, B., Manning, S. W., Niu,
 730 M., Reimer, R. W., Richards, D. A., Scott, E. M., Southon, J. R., Staff, R. A., Turney, C. S. M., and van der
 731 Plicht, J.: IntCal13 and Marine13 Radiocarbon Age Calibration Curves 0–50,000 Years cal BP,
 732 *Radiocarbon*, 55, 1869-1887, 2016.
 733 Richards, D. A. and Dorale, J. A.: Uranium-series chronology and environmental applications of
 734 speleothems, *Uranium-Series Geochemistry*, 52, 407-460, 2003.
 735 Savitzky, A. and Golay, M. J. E.: Smoothing + Differentiation of Data by Simplified Least Squares
 736 Procedures, *Analytical Chemistry*, 36, 1627-8, 1964.
 737 Scholz, D. and Hoffmann, D.: $^{230}\text{Th}/\text{U}$ -dating of fossil reef corals and speleothems, *Quater. Sci. J.*, 57,
 738 52-77, 2008.
 739 Scholz, D. and Hoffmann, D. L.: StalAge - An algorithm designed for construction of speleothem age
 740 models, *Quat. Geochronol.*, 6, 369-382, 2011.
 741 Scholz, D., Mühlinghaus, C., and Mangini, A.: Modelling $\delta^{13}\text{C}$ and $\delta^{18}\text{O}$ in the solution layer on
 742 stalagmite surfaces, *Geochimica et Cosmochimica Acta*, 73, 2592-2602, 2009.
 743 Shi, Z., Allison, S. D., He, Y. J., Levine, P. A., Hoyt, A. M., Beem-Miller, J., Zhu, Q., Wieder, W. R.,
 744 Trumbore, S., and Randerson, J. T.: The age distribution of global soil carbon inferred from radiocarbon
 745 measurements, *Nat. Geosci.*, 13, 555-+, 2020.
 746 Southon, J., Noronha, A. L., Cheng, H., Edwards, R. L., and Wang, Y.: A high-resolution record of
 747 atmospheric ^{14}C based on Hulu Cave speleothem H82, *Quaternary Science Reviews*, 33, 32-41, 2012.
 748 Spötl, C.: Long-term performance of the Gasbench isotope ratio mass spectrometry system for the
 749 stable isotope analysis of carbonate microsamples, *Rapid Communications in Mass Spectrometry*, 25,
 750 1683-1685, 2011.
 751 Spotl, C., Fairchild, I. J., and Tooth, A. F.: Cave air control on dripwater geochemistry, Obir Caves
 752 (Austria): Implications for speleothem deposition in dynamically ventilated caves, *Geochimica Et*
 753 *Cosmochimica Acta*, 69, 2451-2468, 2005.
 754 Spotl, C., Fohlmeister, J., Cheng, H., and Boch, R.: Modern aragonite formation at near-freezing
 755 conditions in an alpine cave, Carnic Alps, Austria, *Chemical Geology*, 435, 60-70, 2016.
 756 Spotl, C. and Mangini, A.: Speleothems and paleoglaciators, *Earth and Planetary Science Letters*, 254,
 757 323-331, 2007.
 758 Spötl, C. and Mangini, A.: Paleohydrology of a high-elevation, glacier influenced karst system in the
 759 central alps (Austria), *Austrian Journal of Earth Sciences*, 103, 92-105, 2010.
 760 Spötl, C., Mangini, A., Bums, S. J., Frank, N., and Pavuza, R.: Speleothems from the high-alpine
 761 Spannagel cave, Zillertal Alps (Austria). In: *Studies of cave sediments*, Springer, 2004.
 762 Spotl, C. and Matthey, D.: Stable isotope microsampling of speleothems for palaeoenvironmental
 763 studies: A comparison of microdrill, micromill and laser ablation techniques, *Chemical Geology*, 235,
 764 48-58, 2006.
 765 Stuiver, M. and Robinson, S. W.: University of Washington GEOSECS north Atlantic carbon-14 results,
 766 *Earth and Planetary Science Letters*, 23, 87-90, 1974.
 767 Therre, S., Fohlmeister, J., Fleitmann, D., Matter, A., Burns, S. J., Arps, J., Schroder-Ritzrau, A., Friedrich,
 768 R., and Frank, N.: Climate-induced speleothem radiocarbon variability on Socotra Island from the Last
 769 Glacial Maximum to the Younger Dryas, *Climate of the Past*, 16, 409-421, 2020.

770 Tochterle, P., Dublyansky, Y., Stobener, N., Mandic, M., and Spotl, C.: High-resolution isotopic
 771 monitoring of cave air CO₂, *Rapid Commun Mass Spectrom*, 31, 895-900, 2017.
 772 Wackerbarth, A., Scholz, D., Fohlmeister, J., and Mangini, A.: Modelling the $\delta^{18}\text{O}$ value of cave drip
 773 water and speleothem calcite, *Earth and Planetary Science Letters*, 299, 387-397, 2010.
 774 Welte, C., Wacker, L., Hattendorf, B., Christl, M., Fohlmeister, J., Breitenbach, S. F., Robinson, L. F.,
 775 Andrews, A. H., Freiwald, A., and Farmer, J. R.: Laser Ablation–Accelerator Mass Spectrometry: An
 776 Approach for Rapid Radiocarbon Analyses of Carbonate Archives at High Spatial Resolution, *Analytical*
 777 *chemistry*, 88, 8570-8576, 2016a.
 778 Welte, C., Wacker, L., Hattendorf, B., Christl, M., Koch, J., Synal, H. A., and Gunther, D.: Novel Laser
 779 Ablation Sampling Device for the Rapid Radiocarbon Analysis of Carbonate Samples by Accelerator
 780 Mass Spectrometry, *Radiocarbon*, 58, 419-435, 2016b.
 781 Welte, C., Wacker, L., Hattendorf, B., Christl, M., Koch, J., Yeman, C., Breitenbach, S. F. M., Synal, H. A.,
 782 and Gunther, D.: Optimizing the analyte introduction for C-14 laser ablation-AMS, *Journal of Analytical*
 783 *Atomic Spectrometry*, 32, 1813-1819, 2017.
 784 Yeman, C., Christl, M., Hattendorf, B., Wacker, L., Welte, C., Brehm, N., and Synal, H. A.: Unravelling
 785 Quasi-Continuous ¹⁴C Profiles by Laser Ablation AMS, *Radiocarbon*, 62, 453-465, 2019.

786

787